Science and Technology Indonesia
e-ISSN:2580-4391 *p*-ISSN:2580-4405
Vol. 6, No. 2, April 2021

Research Paper

Structural Stability of Ni/Al Layered Double Hydroxide Supported on Graphite and Biochar Toward Adsorption of Congo Red

Patimah Mega Syah Bahar Nur Siregar[1], Neza Rahayu Palapa[2], Alfan Wijaya[1], Erni Salasia Fitri[1], Aldes Lesbani[2,3]*

[1] *Department of Chemistry, Faculty of Mathematics and Natural Sciences, Universitas Sriwijaya, Jl. Padang Selasa No. 524 Ilir Barat 1, Palembang-South Sumatera, Indonesia*
[2] *Graduate School, Faculty of Mathematics and Natural Sciences, Universitas Sriwijaya, Jl. Palembang-Prabumulih, Km. 32, Ogan Ilir, South Sumatera, Indonesia*
[3] *Research Center of Inorganic Materials and Complexes, Faculty of Mathematics and Natural Sciences, Universitas Sriwijaya, Jl.Padang Selasa Bukit Besar Palembang 30139, South Sumatera, Indonesia*
***Corresponding author**: aldeslesbani@pps.unsri.ac.id

Abstract
In this research, Ni/Al layered double hydroxide (LDH) was modified by using co-precipitation method to generate Ni/Al-graphite (Ni/Al-GF) and Ni/Al-biochar (Ni/Al-BC). The adsorbents were applied to remove Congo Red from aqueous solution. The obtained samples were characterized by using XRD, FTIR, BET and TG-DTA. The XRD diffraction pattern of Ni/Al LDH, Ni/Al-GF, and Ni/Al-BC presented the formation of composite with decreasing crystallinity. The surface area modified LDHs was higher than the pristine materials, which was obtained 15.106 m^2/g, 21.595 m^2/g and 438.942 m^2/g for Ni/Al-LDH, Ni/Al-GF, Ni/Al-BC respectively. The adsorption of Congo Red on the materials was tested at different parameters and the results exhibited that Congo Red adsorption on LDHs were pseudo-first-order (PFO) kinetic, spontaneous, endothermic and followed Langmuir model. The adsorbents removed Congo Red by high performance stability with adsorption capacity was 116.297 mg/g for Ni/Al-GF and 312.500 mg/g for Ni/Al-BC. These adsorption capacity was higher than the pristine LDH (61.728 mg/g). The regeneration process which carried out for five cycles showed that Ni/Al-GF and Ni/Al-BC have stable structures as reuse adsorbents for Congo Red from aqueous solution.

Keywords
Ni/Al, Biochar, Graphite, Congo Red, Structural Stability

Received: 3 March 2021, Accepted: 7 April 2021
https://doi.org/10.26554/sti.2021.6.2.85-95

1. INTRODUCTION

Dyes are prevalent used in various industries for escelating the polymer properties, to increase the intensity of color in textile industries, and also photography's (Karami et al., 2019). Synthetic dyes are common used in industries such as food, photochemical cell, paper, pharmaceutical, leather tanning industry, hair coloring, and textile industry (Forgacs et al., 2004). Synthetic dyes become popular due to their long durability, more colorful, cheap, and easy to apply (Lellis et al., 2019). However, the dye wastewater disposal generated critical problems because these dyes trigger cancer and mutagenic to human, fauna and flora ecosystem (Khan et al., 2016). Moreover, the process of dyes degradation is running slow, which endanger the environment (Harizi et al., 2018)

Various techniques to remove dyes from wastewater have been applied such as biological, physical and chemical techniques (Duan et al., 2019; Sarkar et al., 2017) photocatalysis (Cantarella et al., 2016; Natarajan et al., 2020), coagulation (Demissie et al., 2021; Gadekar and Ahammed, 2016), adsorption (Puchana-Rosero et al., 2016; Streit et al., 2019). Until this decade, adsorption is the most effective technique to remove dyes from wastewater (Oktriyanti et al., 2019). Adsorption is one of the most important methods to remove pollutants in effluents because low cost, without secondary pollution, high efficiency, and easy operation (Palapa et al., 2019; Zheng et al., 2019).

Adsorption is one of the most important methods to remove pollutants in effluents because of its high efficiency, easy operation, low cost and without secondary pollution. Since the adsorbent has the greatest influence on the adsorption method, it is important to select the appropriate adsorbent for the adsorption in aqueous solution (Hu et al., 2019b). The properties of adsorbent in adsorption process is the most important factor to obtain high adsorption capacity. This is a challenging for researchers to obtain the cheap, eco-sorbent, stable structure, and has good performance to remove pollutants from wastewater.

Congo Red (CR) is one of anionic dyes, which used as color-

ing agent, with chemical formula $C_{32}H_{22}N_6Na_2O_6S_2$ (Khoshsang et al., 2018) as show in Figure 1. CR is stable dye which has good solubility in water and has high endurance to sunlight and temperature (Lei et al., 2017). The existence of aromatic amine groups causes CR as toxic agent that endanger human being and other organisms (Liu et al., 2015b). Adsorption of CR by several adsorbents has been reported by many researchers such as graphite as adsorbent. The adsorption capacity by graphite is 81.301 mg/g (Vinsiah et al., 2020). Hemicelluloses-based magnetic aerogel was efficiently removed CR from aqueous solution with maximum adsorption capacity 137.74 mg/g (Guan et al., 2020). Microalgae Spirulina, sp, was used as biosorbent to remove CR from the aqueous solution with adsorption capacity reaching 0.148 mg/g (Mohadi et al., 2017).

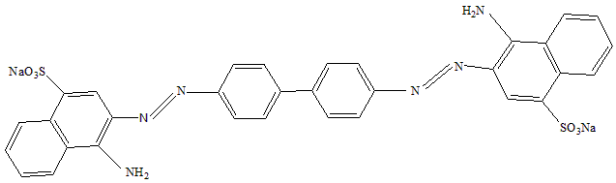

Figure 1. Chemical Structure of CR

The excess of layered double hydroxide (LDH), as adsobent such as easy to synthesize and modify attract many researchers to investigate it extensively. Hu et al., 2019a reported that Ni/Co LDH was applied as an adsorbent to remove CR from aqueous solution with high adsorption capacity of 909.2 mg/g. Sriram et al., 2020 used DE-LDH enhance CR and lead capacity. The adsorption capacity is ten times than the DE as pristine adsorbent.

Cu-Al LDH was synthesized and used as an efficient adsorbent to adsorp CR with adsorption capacity of 120.5 mg/g (Bharali and Deka, 2017). LDHs/cotton fiber composite has an removing CR adsorption capacity twice as large as LDHs. The maximum adsorption capacities of the composite are 232 mg/g and 714 mg/g (Wang et al., 2018). Removal of CR using NMA-LDH and G/NMA-C is conducted with capacity adsorption 156.25 mg/g and 384.62 mg/g (Kazeem et al., 2020).

LDH is well-known material as an anionic layered structure and consists of divalent and trivalent metal cations with general formula $[M_{1-x}^{2+}M_x^{3+}(OH)_2]^{x+}\ A_{x/n}{}^{n-}.mH_2O$, where M^{2+} as divalent and M^{3+} trivalent metal ions and $A_{x/n}{}^{n-}$ as interlayer with n valence (Daud et al., 2019; Stawiński et al., 2018). Due to their unique properties such as large surface areas, high porosity, diverse compositions, excellent anion-exchange capabilities, and high thermal stability, LDHs have been widely used in catalysis, drug delivery and adsorption fields (Wang et al., 2018). Application of LDHs in such areas as catalysts, catalyst' supports, electrode, pharmaceutics, and adsorbents. In order to optimize materials' performances, eforts have been made to vary the composition as well as the particle morphology of the LDHs (Wijitwongwan et al., 2019). LDH could be synthesized with diverse methods as instance hydrothermal, hydrolysis, sonochemical sol-gel and co-precipitation (Bernardo and Ribeiro, 2019; Stawiński et al., 2018). The co-precipitation method is the most common method for synthesize LDHs (Chang et al., 2005). Synthesis of LDH using co-precipitation has resolved as an appealing method because produces high yield with high crystallinity (Palapa et al., 2020; Starukh and Levytska, 2019).

According to Zhang et al., 2019 Mg-Al-CO_3 LDH successfully synthesized by hydrothermal assisted of ultrasound method. Hatami et al., 2018 prepared ZnAl LDHs using hydrolysis treatment and generated LDHs with high crystallinity particle material. Meili et al., 2019 found that LDH-biochar composites which synthesized via co-precipitation to remove dyes with adsorption capacity reaching 406.47 mg/g. Wei et al., 2019 research using In-MOFs LDH which was composited with graphite could remove CR with a maximum capacity of 70.1 mg/g.

In this research, Ni/Al LDH was produced using coprecipita tion methods, which were modified with Biochar (BC) and Graph ite (GF) in order to from generate Ni/Al-BC and Ni/Al-GF. The adsorbents were applied to remove CR from aqueous solution. The obtained materials were characterized by using X-ray diffraction, FTIR, TG-DTA, and BET. The adsorption process was implemented firstly by regeneration process in order to investigate stability of adsorbent follow by kinetic and thermodynamic studies.

2. EXPERIMENTAL SECTION

2.1 Chemicals and Instrumentation

The chemicals used in this work were $Ni(NO_3)_2.6H_2O$ (EMSURE® ACS, 290.81 g/mol, $Al(NO_3)_3.9H_2O$ (Sigma-Aldrich, 375.13 g/mol), HCl (MallinckrodtAR®, 37%), NaOH (EMSURE® ACS, 40 g/mol) and CR. Graphite was obtained from Merck and Biochar is derived from the biomass of rice husk produced through the pyrolysis process. Distilled water was obtained by PT. Bratachem Indonesia. The characterization of materials was performed by X-Ray Rigaku Miniflex- 6000. Characterization of FTIR was conducted using Shimadzu Prestige-21. Analysis BET was performed using Quantachrome Micromeritics. Sample was degassed several times prior analysis. TG-DTA analysis was conducted using Shimadzu TG analyzer by N_2 flow. The concentration of CR was analyzed using UV-Visible spectrophotometer Bio-Base BK-UV1800 at wavelength 516 nm.

2.2 Synthesis of Ni/Al LDH (Wijitwongwan et al., 2019)

Nickel nitrate (17.827 g, 0.01 L) and aluminum nitrate (9.378 g, 0.01 L) with ratio molar Ni/Al (3:1) were mixed then 10 mL of 2 M sodium hydroxide was added to the mixture. The pH of reaction was adjusted to pH 10 by addition of sodium hydroxide. Reaction was kept for 4 hours at 80°C. The solid was then dried in an oven at 100°C for 24 hours. The material was characterized by XRD, FTIR, BET and TGDTA analyses.

2.3 Preparation of Ni/Al-GF and Ni/Al-BC

Composites of Ni/Al-GF and Ni/Al-BC were prepared as similar procedure by (Liu et al., 2015b). Nickel nitrate (2.67 g, 0.015 L) and aluminum nitrate (1.41 g, 0.015 L) was mixed and stirred at room temperature. Then 3 g of graphite or 3 g biochar was added

into reaction mixture following with addition of 2 M sodium hydroxide until pH 10. The mixture is stirred for 72 hours at room temperature to form suspension. The suspension was then heated at 70°C for 24 hours, then filtered and rinsed with distilled water to form Ni/Al-GF or Ni/Al-BC.

2.4 Desorption and Regeneration of Adsorbent

The desorption process was determined to examine the efficiency of the adsorbent. Adsorbent (0.5 g) was added with 50 mL of CR. The mixture was shaken for 120 min. The amount of CR desorbed can be calculated using the equation 1:

$$\% \text{ D} = \frac{C_{ads}}{C_{dsp}} \text{ x } 100\% \quad (1)$$

where, C_{ads} = adsorption concentration; C_{dsp} = desorption capacity after adsorption.

The regeneration efficiency is determined using the equation 2:

$$\% \text{ regeneration} = \frac{Q_r}{Q_0} \text{ x } 100\% \quad (2)$$

where, Q_r = adsorption capacity after regeneration (mg/g); Q_0 = Initial adsorption capacity (mg/g).

The regeneration process of each adsorbent was carried out by adsorbing the CR adsorbed on each adsorbent. CR 100 mg/L as much as 25 mL and each adsorbent of 0.1 g was used for this experiment. After the adsorption process was complete, the absorbance of the CR was measured. The adsorbent was filtered and then dried. These adsorbent will be used for the second and third regeneration process.

2.5 Adsorption Process

The effect of the adsorption kinetics on Ni/Al LDH, BC, GF, Ni/Al-BC and Ni/Al-GF for CR can be determined by varying the adsorption time. CR was added to adsorbent and the mixture was stirred. The adsorption time was evaluated in the range 10-200 minutes. Filtrate was analyzed by UV-Vis spectrophotometer at 516 nm. The adsorption kinetics was studied with the pseudo first order (PFO) and pseudo second order (PSO) using the equation 3 and 4:

$$\log (Q_e - Q_t) = \log Q_e - \left(\frac{k_1}{2.303}\right) t \quad (3)$$

$$\frac{1}{Q_t} = \frac{1}{k_2 Q_e^2} + \frac{1}{Q_e} \quad (4)$$

where, Q_e = adsorption capacity at equilibrium (mg/g); Q_t = adsorption capacity at t (mg/g); T = adsorption time (minute); k_1 = adsorption kinetic rate at pseudo-first-order (minute^{-1}); k_2 = adsorption kinetic rate at pseudo-second-order (g/mg.minute^{-1}).

Adsorption of CR was also studied by variation of initial concentration of CR and adsorption temperature. The adsorption capacity was calculated using equation as follow 5 and 6:

$$\frac{C_e}{Q_e} = \frac{C_e}{Q_m} + \frac{1}{Q_m K_L} \quad (5)$$

$$\text{Log } Q_e = \log K_F + 1/\text{n} \log C_e \quad (6)$$

where, C_e = adsorbate concentration at equilibrium (mg/L); Q_e = adsorption capacity at equilibrium (mg/g); Q_m = maximum adsorption capacity (mg/g); K_L = langmuir isotherm constant; K_F = freundlich constant.

Thermodynamic equations can be calculated from equations 7:

$$\ln K_L = \frac{\Delta S}{R} - \frac{\Delta H}{RT} \quad (7)$$

where, T = temperature (K); R = the gas constant (8.314 J.mol^{-1}.K^{-1}); K_{eq} = the reaction on charge temperature.

The Gibbs energy in the adsorption process was calculated using equation 8:

$$\Delta G^\circ = \Delta H - T\Delta S \quad (8)$$

where, ΔG = gibbs free energy (kJ/mol); ΔH = Enthalpy (kJ/mol); ΔS = Entropy (J/mol K)

3. RESULTS AND DISCUSSION

Based on the XRD pattern in Figure 2(a) Ni/Al LDH has a distinctive peak angle of diffraction at an angle of 2θ = 11.63° (003); 23.00° (006); 35.16° (012); 39.56° (015); 47.4° (018) and 61.59° (110). The results of this XRD pattern analysis are similar to those reported by Li et al., 2010, Ni/Al LDH diffractogram pattern having a sharp peak in the diffraction around the angle of 2θ = 11° (003), 20° (006) and 60° (110) (JCPDS No.15-0087), confirming the successfully preparation of Ni/Al-LDH (Hu et al., 2019b). Ni/Al LDH is then modified to form a composite using biochar and graphite which aims to obtain a material with greater adsorption capacity. Biochar used comes from rice husks and graphite used is standard graphite from Merck which is then characterized using X-ray diffraction as shown in Figures 2(d) and 2(e).

Figure 2(b) showed the diffractogram pattern of the biochar. Bolbol et al., 2019 studied that the diffraction pattern of biochar generally at the peak (002) which indicates the material is amorphous. Figure 2(d) showed the diffractogram pattern of the Ni/Al-BC composite having a diffraction angle of 11.63° which is characteristic of Ni/Al LDH and a diffraction angle of 22.30° which is characteristic of biochar. The XRD graphite pattern is shown in Figure 2(c) with angular diffraction peaks of 2θ at 26.405° (002), 44.50° (101), 54.45° (004) and 77.32° (006). Based on research

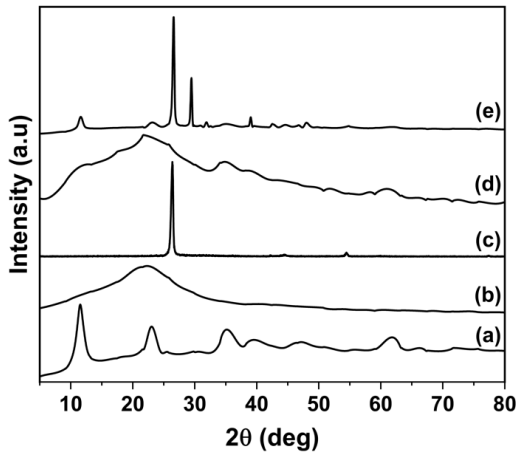

Figure 2. XRD Powder Patterns of Ni/Al LDH (a), BC (b), GF (c), Ni/Al-BC (d), and Ni/Al-GF (e)

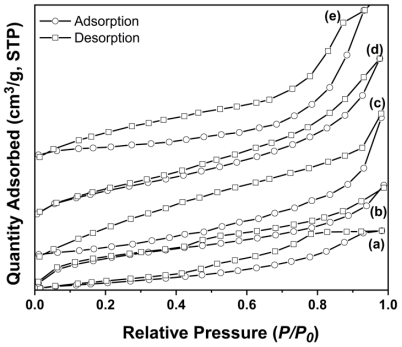

Figure 4. BET Profile of Ni/Al LDH (a), BC (b), GF (c), Ni/Al-BC (d), and Ni/Al-GF (e)

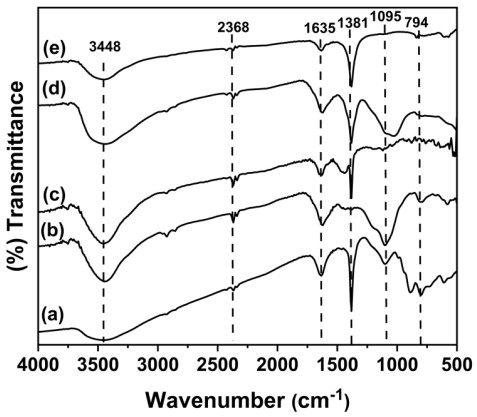

Figure 3. FTIR Spectrum of Ni/Al LDH (a), BC (b), GF (c), Ni/Al-BC (d), and Ni/Al-GF (e)

conducted by Popova, 2017, the diffractogram pattern that appears on graphite is at an angle of 2θ 26.5° (002); 54.7° (004); and 87.1° (006) (JCPDS No.75-1621) (Pakhira et al., 2016). Figure 2(e) showed the diffraction peaks of Ni/Al LDH and graphite appear in the Ni/Al-GF composite.

Figure 3(a) shows the vibrational peak of Ni/Al LDH which shows a vibration peak at wavenumber 3464 cm^{-1} indicating the presence of O-H vibrations from water molecules. The peak of the vibration at wavenumber 1635 cm^{-1} indicates a bending vibration of O-H. The peak of the vibration at wavenumber 1381 cm^{-1} indicates the existence of vibration from the NO_3^- anion and the peak of the vibration at wavenumber 748 cm^{-1} is the M-O vibration in the form of Ni-O and Al-O. Figure 3(b) showed the FTIR spectrum of biochar with a vibration peak at wavenumber 3448 cm^{-1} indicating the presence of O-H vibrations. The peak of the vibration at wavenumber 1620 cm^{-1} indicates a C=C vibration. The peak vibration at wavenumber 1103 cm^{-1} indicates the presence of Si-O-Si and the peak vibration at wavenumber 470 cm^{-1} indicates the existence of Al-O vibrations. According to Lazzari et al., 2018 the FTIR spectrum of these biochar is similar even though the absorption intensity varies.

Figure 3(c) shows the graphite spectrum. The vibration pattern that is formed at the wavenumber 3402 cm^{-1} indicates the presence of –OH bonds in the water molecules contained in the material. Other vibration pattern that appears are at the wavenumbers 1635 cm^{-1} and 1381 cm^{-1} which indicates the presence of C=C and C-H bonds in graphite. Kartick et al., 2013 reported that the graphite vibrational pattern appeared at wavenumber 1562 and 3434 cm^{-1} which indicated the presence of a C=C bond and an –OH bond. Figure 3(d) shows the typical vibrational peak of Ni/Al LDH and typical vibration peaks of rice husk biochar. Figure 3(e) shows the similarity of FTIR patterns on Ni/Al LDH and graphite, this shows that the composite material from Ni/Al LDH and graphite was successfully prepared.

The nitrogen adsorption-desorption isotherm of composites and starting materials is shown in Figure 4 and BET measurement data is presented in Table 1. The adsorption desorption curve showed all materials has similar isotherm type and hysteresis was observed. The isotherm pattern that does not overlap between the adsorption and desorption charts shows that all of these materials are classified as type IV adsorption-desorption isotherms.

Table 1 shows that Ni/Al-BC and Ni/Al-GF have a larger surface area than the pristine material. The surface area of Ni/Al-BC has increased up to twenty nine times and Ni/Al-GF has slightly increased compared to the pure material.

Figure 5 shows the thermal analysis of all materials. Figure 5(a) shows that at temperature 100°C there is loss of water

Table 1. BET Analysis of Materials

Materials	Surface Area (m^2/g)	Pore Size (nm), BJH	Pore Volume (cm^2/g)BJH
Ni/Al LDH	15.106	2.897	0.043
BC	50.936	12.089	0.025
GF	11.558	3.169	0.027
Ni/Al-BC	438.942	12.301	0.002
Ni/Al-GF	21.595	3.153	0.034

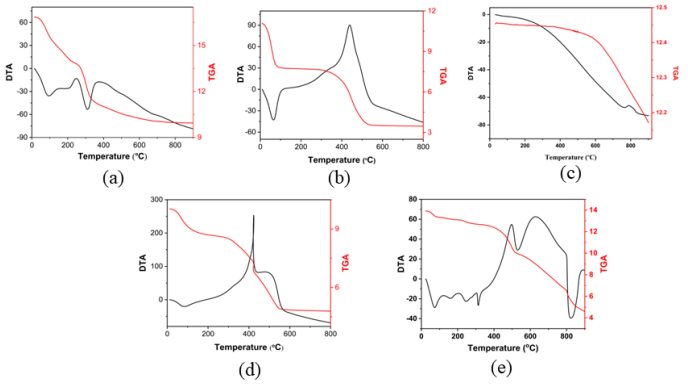

Figure 5. Thermal Profile of Ni/Al LDH (a), BC (b), GF (c), Ni/Al-BC (d), and Ni/Al-GF (e)

molecules on the surface of LDH. The endothermic peak at temperature 300°C show the loss of nitrate molecules on the Ni/Al LDH interlayer. Figure 5(b) shows the exothermic peak of BC at 420°C shows that biochar releases energy and a horizontal line at 600°C shows that the biochar has been completely oxidized. Figures 5(c) shows that at a temperature of 760°C the material has become graphite oxide. The composite shown in Figure 5(d) and 5(e) had two kinds peaks i.e. endothermic and exothermic.

The desorption process of the adsorbent is carried out using several reagents (water, hydrochloric acid, sodium hydroxide, and ethanol). The desorption result of each adsorbent is shown in Figure 6. The results in figure 6 show that the hydrochloric

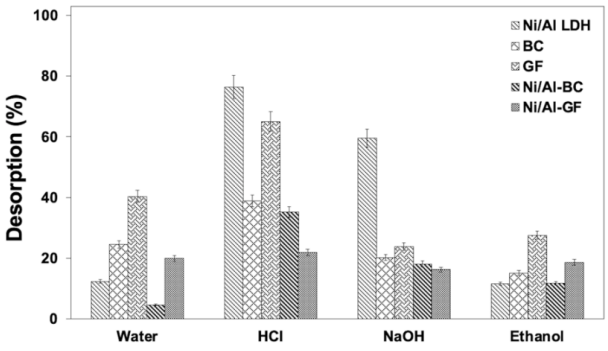

Figure 6. Desorption of Adsorbent

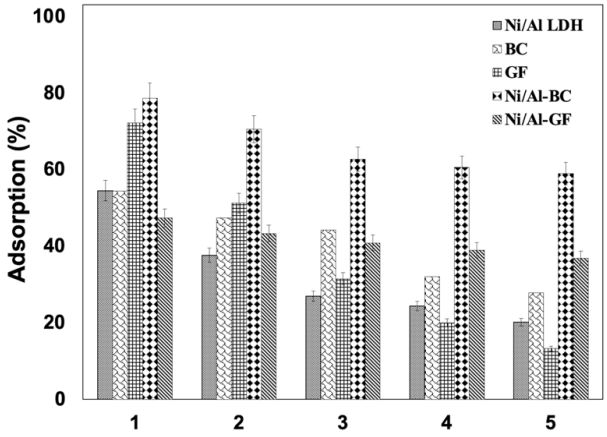

Figure 7. Regeneration of Adsorbent

acid can desorp CR higher than other reagents. This is due to the H^+ ions from acid can release anions from the CR dye through the interaction between acid and adsorbent. After the desorption process is carried out, the adsorbent is used for the regeneration process.

Figure 7 shows the regeneration processes of Ni/Al-BC and Ni/Al-GF are more stable and have a greater adsorption capacity than the pristine material. Adsorption on Ni/Al-BC at five re-adsorption process was achieved up to 78-58%. Adsorption capacity on Ni/Al-GF was low but the re-adsorption process until five times process resulted almost similar adsorption capacity in the range 47-36%. In the regeneration process Ni/Al-BC has a greater adsorption capacity than Ni/Al-GF, this is due to an increase in the surface area of Ni/Al-BC reaching 20 times. The adsorption capacity of BC and GF also experienced a decrease in adsorption capacity and structural stability. This is because the organic material is not stable to the adsorption-desorption process. So it can be concluded that the formation of composites with materials derived from carbon can increase the stability of the Ni/Al LDH structure.

Ni/Al LDH, BC, GF, Ni/Al-BC and Ni/Al-GF were used as adsorbent for adsorption of CR. Firstly, the kinetics parameters were studied through the effect of the adsorption contact time as shown in Figure 8 and Table 2. Figure 8 shows that the adsorption of CR reached equilibrium at 120 minutes. The CR adsorption process follows the kinetics parameters of PFO adsorption with a correlation coefficient (R^2) close to unity. In addition, the calculation of adsorption capacity (q_e) given by the PFO is very close to the empirical adsorption capacity (q_{exp}). As the results are shown in Table 2.

Secondly, the thermodynamic parameters were studied thro ugh variations in initial CR concentration and adsorption temperature. Figure 9 shows that the adsorption capacity increases with the increasing effect of temperature on the adsorption process.

Based on the value of the maximum adsorption capacity (Q_m) presented in Table 3, the highest yield on the Ni/Al-BC composite adsorbent was 312.500 mg/g. This indicates that the adsorption

Table 2. Kinetic Parameter

Adsorbent	Initial Concentration (mg/L)	Qe_{exp} (mg/g)	PFO			PSO		
			Qe_{calc} (mg/g)	R^2	k_1	Qe_{calc} (mg/g)	R^2	k_2
Ni/Al LDH	99.429	31.111	33.674	0.992	0.026	2.282	0.878	0.222
BC	99.429	35.996	21.296	0.957	0.025	2.325	0.910	0.202
GF	99.429	30.682	42.954	0.972	0.049	34.602	0.993	0.001
Ni/Al-BC	99.429	51.746	57.003	0.988	0.026	3.634	0.944	0.155
Ni/Al-GF	99.429	32.046	16.638	0.901	0.022	35.587	0.992	0.001

Table 3. Isotherm Adsorption

Adsorbent	Adsorption Isotherm	Adsorption Constant	T			
			30˚C	40˚C	50˚C	60˚C
Ni/Al LDH	Langmuir	Q_{max}	42.194	54.348	58.823	61.728
		k_L	0.148	0.104	0.126	0.19
		R^2	0.994	0.987	0.993	0.999
	Freundlich	n	6.968	2.047	7.326	5.988
		k_F	21.125	7.941	29.771	29.471
		R^2	0.694	0.964	0.868	0.899
BC	Langmuir	Q_{max}	42.735	42.918	42.735	42.735
		k_L	0.044	0.031	0.057	0.064
		R^2	0.979	0.98	0.982	0.989
	Freundlich	n	2.82	1.427	1.159	1.263
		k_F	7.323	2.734	1.943	2.69
		R^2	0.959	0.99	0.962	0.958
GF	Langmuir	Q_{max}	81.301	82.645	86.207	87.719
		k_L	0.267	0.367	0.411	0.648
		R^2	0.999	0.999	0.999	0.999
	Freundlich	n	1.248	1.543	1.642	2.232
		k_F	1.492	1.507	1.517	1.532
		R^2	0.941	0.930	0.971	0.967
Ni/Al-GF	Langmuir	Q_{max}	98.039	105.263	112.36	116.297
		k_L	0.027	0.03	0.033	0.041
		R^2	0.975	0.973	0.965	0.963
	Freundlich	n	1.916	1.911	1.897	1.948
		k_F	6.925	7.82	8.704	10.359
		R^2	0.966	0.961	0.949	0.937
Ni/Al-BC	Langmuir	Q_{max}	136.986	163.934	250	312.5
		k_L	0.036	0.011	0.028	1
		R^2	0.931	0.952	0.964	0.9999
	Freundlich	n	14.97	19.763	10.977	12.706
		k_F	40.804	47.315	41.352	46.452
		R^2	0.965	0.921	0.904	0.999

Table 4. Thermodynamic Adsorption

Adsorbent	T (K)	Q_e (mg/g)	ΔH (kJ/mol)	ΔS (J/mol K)	ΔG (kJ/mol)
Ni/Al LDH	303	36.899	21.924	0.071	-0.415
	313	45.506			-0.295
	323	49.304			-1.005
	333	53.228			-1.715
BC	303	45.429	4.853	0.016	-0.004
	313	46.778			-0.165
	323	47.968			-0.325
	333	49.397			-0.485
GF	303	50.429	20.487	0.074	-1.872
	313	53.683			-2.61
	323	56.857			-3.348
	333	60.587			-4.086
Ni/Al-GF	303	64.515	16.018	0.053	-0.115
	313	70.197			-0.648
	323	76.106			-1.18
	333	81.863			-1.713
Ni/Al-BC	303	51.709	12.961	0.047	-1.358
	313	56.392			-1.831
	323	58.291			-2.303
	333	60.316			-2.776

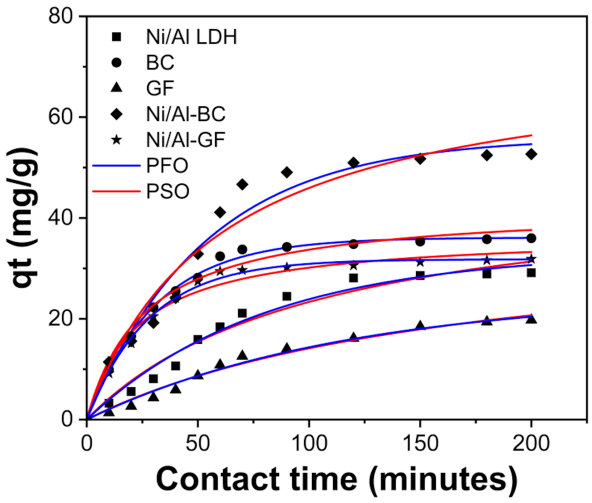

Figure 8. Time Variation of Adsorption

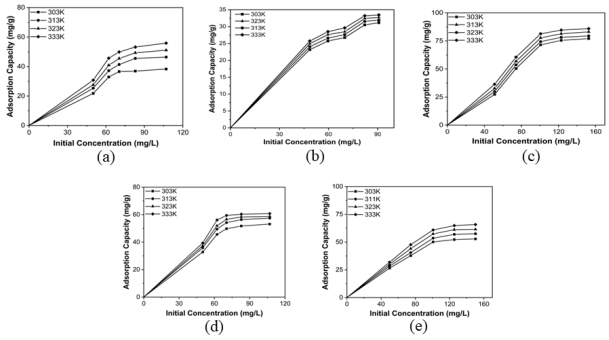

Figure 9. Effect of Adsorption Time on Ni/Al LDH (a), BC (b), GF (c), Ni/Al-BC (d), and Ni/Al-GF (e)

process of CR is more effective using Ni/Al-BC composites. Based on Arabpour et al., 2021 the determination of the adsorption isotherm model is determined from the linear regression value close to 1. In Table 3 shows that the linear regression value of each adsorbent tends to follow the Langmuir isotherm model. According to the Langmuir isotherm model, Aichour et al., 2019 explains that the adsorption process occurs monolayer, stipulates that adsorption process happens on the homogeneous adsorbent surface with similar adsorption energy for all molecules.

Gibbs free energy (ΔG) is one of the thermodynamic parameters used to determine whether an adsorption process is spontaneous or not. The ΔG value data showed that all are negative, which means that the adsorption is spontaneous. The enthalpy value (ΔH) is the total change in heat energy that occurs during the adsorption process. If the ΔH value is negative, the adsorption process is exothermic, where the heat of the reaction is transferred from the system to the environment. If ΔH is positive, the adsorption process is endothermic in that heat is transferred from the environment to the system. The results showed that the ΔH value is below +40 kJ/mol, which indicates that the adsorption process of CR is endothermic. The entropy value (ΔS) displayed showed the parameter of the degree of irregularity that occurs in the system. Where the greater the dye concentration used, the smaller the degree of irregularity.

Table 5. Adsorption of CR by Several Adsorbents

Adsorbent	Adsorption capacity (mg/g)	Reference
Mg/Al hydrotalcite	22.222	(Said and Palapa, 2017)
Phyrophyllite	4	(Amran and Zulfikar, 2010)
Mg-Al LDH	23.02	(Sriram et al., 2020)
Compost	5.33	(Kristanto et al., 2018)
Gulmohar Leaf Powder	434.7	(Keskin et al., 2018)
Phoenix Dactylifera Seeds	61.72	(Pathania et al., 2016)
Xanthan Gum/Silica Hybrid	209.205	(Ghorai et al., 2013)
Activated Carbon Prepared From Coir Pith	6.7	(Namasivayam and Kavitha, 2002)
PVA/SA/ZSM-5 Zeolite Membrane	19	(Radoor et al., 2020)
Acid-Activated Bentonite	20.7	(Taher et al., 2019)
Soybean Curd	69.9	(Zhang et al., 2018)
Organified Mixture Of Illite-Kaolinite	83	(Omer et al., 2018)
Polystyrene Microspheres	18	(Chen et al., 2019)
SnO_2-80 nanoparticles	43.291	(Abdelkader et al., 2015)
shiitake mushroom	217.86	(Yang et al., 2019)
Titanium Dioxide	152	(Abbas, 2020)
TiO_2-Sulfonated	36.5	(Widiyowati et al., 2020)
Magnetic $Ni_{0.5}Zn_{0.5}Fe_2O_4$ nanopowders	40.5	(Liu et al., 2015a)
Banana peel	18.2	(Annadurai et al., 2002)
Orange peel	14	(Annadurai et al., 2002)
Ni/Al LDH	61.728	This Research
BC	42.735	This Research
GF	87.719	This Research
Ni/Al-BC	312.5	This Research
Ni/Al-GF	116.297	This Research

Adsorption of CR using adsorbent produces a positive ΔS value with a small value. This shows that the degree of irregularity and interaction of the adsorbent with CR in aqueous solution has a small interaction. Table 5 shows the adsorption of CR using several adsorbents. The adsorption capacity of CR in this research is quite similar with previous reported literatures.

4. CONCLUSIONS

The development of Ni/Al LDH with carbon-based support materials in the form of biochar and graphite has been successfully synthesized. This is evidenced from the results of the main characterization in the form of XRD showing the appearance of LDH diffraction at an angle of 2θ = 11 with the diffraction plane (003) which indicates the characteristics of the layered material. Ni/Al-BC composites showed biochar characteristics at a diffraction angle of 2θ = 23 and Ni/Al-GF composites showed graphite characteristics at a diffraction angle of 2θ = 26. The surface area of Ni/Al-BC 438.942 m^2/g was largely higher than Ni/Al-GF 21.595 m^2/g. The adsorbents removed CR with adsorption capacity of about 116.297 mg/g for Ni/Al-GF and 312.500 mg/g for Ni/Al-BC. The regeneration process which carried out for five cycles showed that Ni/Al-GF and Ni/Al-BC have stable structures as reuse adsorbents of CR adsorption.

5. ACKNOWLEDGEMENT

Authors thanks to Universitas Sriwijaya for support this research by Hibah Profesi contract No. 0687/UN9/SK.BUK.KP/2020. This article is additional output of these whole project. Authors also thanks to Research Center of Inorganic Materials and Complexes FMIPA Universitas Sriwijaya for laboratory analysis.

REFERENCES

Abbas, M. (2020). Experimental investigation of titanium dioxide as an adsorbent for removal of Congo red from aqueous solution, equilibrium and kinetics modeling. *Journal of Water Reuse and Desalination*, **10**(3); 251–266

Abdelkader, E., L. Nadjia, and V. Rose-Noëlle (2015). Adsorption of Congo red azo dye on nanosized SnO2 derived from sol-gel method. *International Journal of Industrial Chemistry*, **7**(1); 53–70

Aichour, A., H. Zaghouane-Boudiaf, F. B. M. Zuki, M. K. Aroua, and C. V. Ibbora (2019). Low-cost, biodegradable and highly effective adsorbents for batch and column fixed bed adsorption processes of methylene blue. *Journal of Environmental Chemical Engineering*, **7**(5); 103409

Amran, M. B. and M. A. Zulfikar (2010). Removal of Congo Red

dye by adsorption onto phyrophyllite. *International Journal of Environmental Studies*, **67**(6); 911–921

Annadurai, G., R. Juang, and D. Lee (2002). Use of cellulose-based wastes for adsorption of dyes from aqueous solutions. *Journal of Hazardous Materials*, **92**(3); 263–274

Arabpour, A., S. Dan, and H. Hashemipour (2021). Preparation and optimization of novel graphene oxide and adsorption isotherm study of methylene blue. *Arabian Journal of Chemistry*, **14**(3); 103003

Bernardo, M. P. and C. Ribeiro (2019). Zn–Al-based layered double hydroxides (LDH) active structures for dental restorative materials. *Journal of Materials Research and Technology*, **8**(1); 1250–1257

Bharali, D. and R. C. Deka (2017). Adsorptive removal of congo red from aqueous solution by sonochemically synthesized NiAl layered double hydroxide. *Journal of Environmental Chemical Engineering*, **5**(2); 2056–2067

Bolbol, H., M. Fekri, and M. Hejazi-Mehrizi (2019). Layered double hydroxide–loaded biochar as a sorbent for the removal of aquatic phosphorus: behavior and mechanism insights. *Arabian Journal of Geosciences*, **12**(16); 1–11

Cantarella, M., R. Sanz, M. A. Buccheri, F. Ruffino, G. Rappazzo, S. Scalese, G. Impellizzeri, L. Romano, and V. Privitera (2016). Immobilization of nanomaterials in PMMA composites for photocatalytic removal of dyes, phenols and bacteria from water. *Journal of Photochemistry and Photobiology A: Chemistry*, **321**; 1–11

Chang, Z., D. Evans, X. Duan, C. Vial, J. Ghanbaja, V. Prevot, M. de Roy, and C. Forano (2005). Synthesis of [Zn–Al–CO3] layered double hydroxides by a coprecipitation method under steady-state conditions. *Journal of Solid State Chemistry*, **178**(9); 2766–2777

Chen, W., Y. Shen, Y. Ling, Y. Peng, M. Ge, and Z. Pan (2019). Synthesis of Positively Charged Polystyrene Microspheres for the Removal of Congo Red, Phosphate, and Chromium(VI). *ACS Omega*, **4**(4); 6669–6676

Daud, M., A. Hai, F. Banat, M. B. Wazir, M. Habib, G. Bharath, and M. A. Al-Harthi (2019). A review on the recent advances, challenges and future aspect of layered double hydroxides (LDH) – Containing hybrids as promising adsorbents for dyes removal. *Journal of Molecular Liquids*, **288**; 110989

Demissie, H., G. An, R. Jiao, T. Ritigala, S. Lu, and D. Wang (2021). Modification of high content nanocluster-based coagulation for rapid removal of dye from water and the mechanism. *Separation and Purification Technology*, **259**; 117845

Duan, C., X. Meng, C. Liu, W. Lu, J. Liu, L. Dai, W. Wang, W. Zhao, C. Xiong, and Y. Ni (2019). Carbohydrates-rich corncobs supported metal-organic frameworks as versatile biosorbents for dye removal and microbial inactivation. *Carbohydrate Polymers*, **222**; 115042

Forgacs, E., T. Cserháti, and G. Oros (2004). Removal of synthetic dyes from wastewaters: a review. *Environment International*, **30**(7); 953–971

Gadekar, M. R. and M. M. Ahammed (2016). Coagulation/flocculation process for dye removal using water treatment residuals: modelling through artificial neural networks. *Desalination and Water Treatment*, **57**(55); 26392–26400

Ghorai, S., A. K. Sarkar, A. B. Panda, and S. Pal (2013). Effective removal of Congo red dye from aqueous solution using modified xanthan gum/silica hybrid nanocomposite as adsorbent. *Bioresource technology*, **144**; 485–491

Guan, Y., J. Rao, Y. Wu, H. Gao, S. Liu, G. Chen, and F. Peng (2020). Hemicelluloses-based magnetic aerogel as an efficient adsorbent for Congo red. *International Journal of Biological Macromolecules*, **155**; 369–375

Harizi, I., D. Chebli, A. Bouguettoucha, S. Rohani, and A. Amrane (2018). A New Mg–Al–Cu–Fe-LDH Composite to Enhance the Adsorption of Acid Red 66 Dye: Characterization, Kinetics and Isotherm Analysis. *Arabian Journal for Science and Engineering*, **44**(6); 5245–5261

Hatami, H., A. Fotovat, and A. Halajnia (2018). Comparison of adsorption and desorption of phosphate on synthesized Zn-Al LDH by two methods in a simulated soil solution. *Applied Clay Science*, **152**; 333–341

Hu, H., J. Liu, Z. Xu, L. Zhang, B. Cheng, and W. Ho (2019a). Hierarchical porous Ni/Co-LDH hollow dodecahedron with excellent adsorption property for Congo red and Cr(VI) ions. *Applied Surface Science*, **478**; 981–990

Hu, X., P. Li, X. Zhang, B. Yu, C. Lv, N. Zeng, J. Luo, Z. Zhang, J. Song, and Y. Liu (2019b). Ni-Based Catalyst Derived from NiAl Layered Double Hydroxide for Vapor Phase Catalytic Exchange between Hydrogen and Water. *Nanomaterials*, **9**(12); 1688

Karami, Z., M. Jouyandeh, S. M. Hamad, M. R. Ganjali, M. Aghazadeh, L. Torre, D. Puglia, and M. R. Saeb (2019). Curing epoxy with Mg-Al LDH nanoplatelets intercalated with carbonate ion. *Progress in Organic Coatings*, **136**; 105278

Kartick, B., S. K. Srivastava, , and I. Srivastava (2013). Green Synthesis of Graphene. *Journal of Nanoscience and Nanotechnology*, **13**(6); 4320–4324

Kazeem, T. S., M. Zubair, M. Daud, and M. A. Al-Harthi (2020). Enhanced Removal of Eriochrome Black T Using Graphene/NiMgAl-Layered Hydroxides: Isotherm, Kinetic, and Thermodynamic Studies. *Arabian Journal for Science and Engineering*; 1–15

Keskin, E., U. Solmaz, G. Binzet, I. Gumus, and H. Arslan (2018). Synthesis, characterization and crystal structure of platinum (II) complexes with thiourea derivative ligands. *European Journal of Chemistry*, **9**(4); 360–368

Khan, S. A., S. B. Khan, and A. M. Asiri (2016). Toward the design of Zn–Al and Zn–Cr LDH wrapped in activated carbon for the solar assisted de-coloration of organic dyes. *RSC Advances*, **6**(86); 83196–83208

Khoshsang, H., A. Ghaffarinejad, H. Kazemi, Y. Wang, and H. Arandiyan (2018). One-pot synthesis of S-doped Fe 2 O 3/C magnetic nanocomposite as an adsorbent for anionic dye removal: equilibrium and kinetic studies. *Journal of Nanostructure in Chemistry*, **8**(1); 23–32

Kristanto, G. A., A. R. Lamurvie, and W. Koven (2018). A Study of Compost as an Adsorbent for Congo Red Dye Removal

Process. *Reaktor*, **17**(4); 203

Lazzari, E., T. Schena, M. C. A. Marcelo, C. T. Primaz, A. N. Silva, M. F. Ferrão, T. Bjerk, and E. B. Caramão (2018). Classification of biomass through their pyrolytic bio-oil composition using FTIR and PCA analysis. *Industrial Crops and Products*, **111**; 856–864

Lei, C., M. Pi, C. Jiang, B. Cheng, and J. Yu (2017). Synthesis of hierarchical porous zinc oxide (ZnO) microspheres with highly efficient adsorption of Congo red. *Journal of Colloid and Interface Science*, **490**; 242–251

Lellis, B., C. Z. Fávaro-Polonio, J. A. Pamphile, and J. C. Polonio (2019). Effects of textile dyes on health and the environment and bioremediation potential of living organisms. *Biotechnology Research and Innovation*, **3**(2); 275–290

Li, K., N. Kumada, Y. Yonesaki, T. Takei, N. Kinomura, H. Wang, and C. Wang (2010). The pH effects on the formation of Ni/Al nitrate form layered double hydroxides (LDHs) by chemical precipitation and hydrothermal method. *Materials Chemistry and Physics*, **121**(1-2); 223–229

Liu, R., H. Fu, H. Yin, P. Wang, L. Lu, and Y. Tao (2015a). A facile sol combustion and calcination process for the preparation of magnetic Ni0.5Zn0.5Fe2O4 nanopowders and their adsorption behaviors of Congo red. *Powder Technology*, **274**; 418–425

Liu, X., W. Li, N. Chen, X. Xing, C. Dong, and Y. Wang (2015b). Ag–ZnO heterostructure nanoparticles with plasmon-enhanced catalytic degradation for Congo red under visible light. *RSC Advances*, **5**(43); 34456–34465

Meili, L., P. Lins, C. Zanta, J. Soletti, L. Ribeiro, C. Dornelas, T. Silva, and M. Vieira (2019). MgAl-LDH/Biochar composites for methylene blue removal by adsorption. *Applied Clay Science*, **168**; 11–20

Mohadi, R., , Z. Hanafiah, H. Hermansyah, and H. Zulkifli (2017). Adsorption of procion red and congo red dyes using microalgae Spirulina sp. *Science and Technology Indonesia*, **2**(4); 102–104

Namasivayam, C. and D. Kavitha (2002). Removal of Congo Red from water by adsorption onto activated carbon prepared from coir pith, an agricultural solid waste. *Dyes and pigments*, **54**(1); 47–58

Natarajan, S., V. Anitha, G. P. Gajula, and V. Thiagarajan (2020). Synthesis and Characterization of Magnetic Superadsorbent Fe3O4-PEG-Mg-Al-LDH Nanocomposites for Ultrahigh Removal of Organic Dyes. *ACS Omega*, **5**(7); 3181–3193

Oktriyanti, M. M., N. R. Palapa, R. Mohadi, and A. Lesbani (2019). Modification Of Zn-Cr Layered Double Hydroxide With Keggin Ion [?-SiW12O40] 4-AS Cr (VI) Adsorbent. *Indonesian Journal of Environmental Management and Sustainability*, **3**(3); 93–99

Omer, O. S., B. H. Hussein, A. M. Ouf, M. A. Hussein, and A. Mgaidi (2018). An organified mixture of illite-kaolinite for the removal of Congo red from wastewater. *Journal of Taibah University for Science*, **12**(6); 858–866

Pakhira, B., M. Ghosh, A. Allam, and S. Sarkar (2016). Carbon nano onions cross the blood brain barrier. *RSC advances*, **6**(35); 29779–29782

Palapa, N. R., R. Mohadi, A. Rachmat, and A. Lesbani (2020). Adsorption Study of Malachite Green Removal from Aqueous Solution Using Cu/M3+ (M3+=Al, Cr) Layered Double Hydroxide. *Mediterranean Journal of Chemistry*, **10**(1); 33–45

Palapa, N. R., T. Taher, R. Mohadi, and A. Lesbani (2019). Removal of Anionic Direct Dye Using Zn/Al, Zn/Fe and Zn/Cr Layered Double Hydroxides Toward Interlayer Distance. *Science and Technology Indonesia*, **4**(3); 70

Pathania, D., A. Sharma, and Z.-M. Siddiqi (2016). Removal of congo red dye from aqueous system using Phoenix dactylifera seeds. *Journal of Molecular Liquids*, **219**; 359–367

Popova, A. N. (2017). Crystallographic analysis of graphite by X-Ray diffraction. *Coke and Chemistry*, **60**(9); 361–365

Puchana-Rosero, M., M. A. Adebayo, E. C. Lima, F. M. Machado, P. S. Thue, J. C. Vaghetti, C. S. Umpierres, and M. Gutterres (2016). Microwave-assisted activated carbon obtained from the sludge of tannery-treatment effluent plant for removal of leather dyes. *Colloids and Surfaces A: Physicochemical and Engineering Aspects*, **504**; 105–115

Radoor, S., J. Karayil, J. Parameswaranpillai, and S. Siengchin (2020). Removal of anionic dye Congo red from aqueous environment using polyvinyl alcohol/sodium alginate/ZSM-5 zeolite membrane. *Scientific Reports*, **10**; 1–15

Said, M. and N. R. Palapa (2017). Adsorption of congo red using Mg/Al hydrotalcite. *Science & Technology Indonesia*, **1**(2); 17–21

Sarkar, S., A. Banerjee, U. Halder, R. Biswas, and R. Bandopadhyay (2017). Degradation of Synthetic Azo Dyes of Textile Industry: a Sustainable Approach Using Microbial Enzymes. *Water Conservation Science and Engineering*, **2**(4); 121–131

Sriram, G., U. T. Uthappa, D. Losic, M. Kigga, H.-Y. Jung, and M. D. Kurkuri (2020). Mg–Al-Layered Double Hydroxide (LDH) Modified Diatoms for Highly Efficient Removal of Congo Red from Aqueous Solution. *Applied Sciences*, **10**(7); 2285

Starukh, H. and S. Levytska (2019). The simultaneous anionic and cationic dyes removal with Zn Al layered double hydroxides. *Applied Clay Science*, **180**; 105183

Stawiński, W., A. Węgrzyn, G. Mordarski, M. Skiba, O. Freitas, and S. Figueiredo (2018). Sustainable adsorbents formed from by-product of acid activation of vermiculite and leached-vermiculite-LDH hybrids for removal of industrial dyes and metal cations. *Applied Clay Science*, **161**; 6–14

Streit, A. F., L. N. Côrtes, S. P. Druzian, M. Godinho, G. C. Collazzo, D. Perondi, and G. L. Dotto (2019). Development of high quality activated carbon from biological sludge and its application for dyes removal from aqueous solutions. *Science of The Total Environment*, **660**; 277–287

Taher, T., D. Rohendi, R. Mohadi, and A. Lesbani (2019). Congo red dye removal from aqueous solution by acid-activated bentonite from sarolangun: kinetic, equilibrium, and thermodynamic studies. *Arab Journal of Basic and Applied Sciences*, **26**(1); 125–136

Vinsiah, R., R. Mohadi, and A. Lesbani (2020). Performance of Graphite for Congo Red and Direct Orange Adsorption. *Indonesian Journal of Environmental Management and Sustain-*

ability, **4**(4); 125–132

Wang, X., W. Zhou, C. Wang, and Z. Chen (2018). Cotton fiber-supported layered double hydroxides for the highly efficient adsorption of anionic organic pollutants in water. *New Journal of Chemistry*, **42**(12); 9463–9471

Wei, F.-H., Q. hui Ren, Z. Liang, and D. Chen (2019). Synthesis of Graphene Oxide/Metal-Organic Frameworks Composite Materials for Removal of Congo Red from Wastewater. *ChemistrySelect*, **4**(19); 5755–5762

Widiyowati, I. I., M. Nurhadi, M. Hatami, and L. S. Yuan (2020). Effective TiO2-Sulfonated Carbon-derived from Eichhornia crassipes in The Removal of Methylene Blue and Congo Red Dyes from Aqueous Solution. *Bulletin of Chemical Reaction Engineering & Catalysis*, **15**(2); 476–489

Wijitwongwan, R. P., S. G. Intasa-ard, M. Ogawa, et al. (2019). Preparation of layered double hydroxides toward precisely designed hierarchical organization. *ChemEngineering*, **3**(3); 68

Yang, K., Y. Li, H. Zheng, X. Luan, H. Li, Y. Wang, Q. Du, K. Sui, H. Li, and Y. Xia (2019). Adsorption of Congo red with hydrothermal treated shiitake mushroom. *Materials Research Express*, **7**(1); 015103

Zhang, W., Y. Liang, J. Wang, Y. Zhang, Z. Gao, Y. Yang, and K. Yang (2019). Ultrasound-assisted adsorption of Congo red from aqueous solution using Mg Al CO3 layered double hydroxide. *Applied Clay Science*, **174**; 100–109

Zhang, Z., Y. Li, Q. Du, and Q. Li (2018). Adsorption of Congo Red from Aqueous Solutions by Porous Soybean Curd Xerogels. *Polish Journal of Chemical Technology*, **20**(3); 95–102

Zheng, Y., B. Cheng, W. You, J. Yu, and W. Ho (2019). 3D hierarchical graphene oxide-NiFe LDH composite with enhanced adsorption affinity to Congo red, methyl orange and Cr(VI) ions. *Journal of Hazardous Materials*, **369**; 214–225

